## RÓYAL SOCIETY OF CHEMISTRY

## **Journal Name**

## **ARTICLE**

# Magnetic anisotropy and slow magnetic relaxation processes of cobalt(II)-pseudohalide complexes

Hui-Hui Cui, a Yi-Quan Zhang, b Xue-Tai Chen, a Zhenxing Wang, c, and Zi-Ling Xued

Received 00th January 20xx, Accepted 00th January 20xx

DOI: 10.1039/x0xx00000x

www.rsc.org/

Three mononuclear six-coordinate Co(II)-pseudohalide complexes  $[Co(L)X_2]$  with two N-donor pseudohalido coligands occupying in the cis-positions (X is NCS<sup>-</sup>(1),NCSe<sup>-</sup>(2) or N(CN)<sub>2</sub><sup>-</sup>(3)), and a five-coordinate complex  $[Co(L)(NCO)][B(C_6H_5)_4]$  (4), where L is a macrocyclic ligand,1, 4, 7, 10-tetramethyl-1, 4, 7, 10-tetraazacyclododecane (12TMC), have been prepared and structurally characterized. Easy-plane magnetic anisotropies for 1-3 and easy-axis anisotropy for 4 were revealed via the analyses of the direct-current magnetic data, high–frequency and –field EPR (HFEPR) spectra and ab initio theoretical calculations. They have found to display slow magnetic relaxations and thus are field-induced single-molecule magnets. Typically, 1 and 2 show two slow relaxation processes under an external dc field, in agreement with two crystallographically different molecules in the crystal lattice, while only one relaxation process occurs in 3 and 4. The Raman-like mechanism is found to be dominant in the studied temperature in 1, while the Orbach mechanism contrubute to some extent at high temperature range besides the dominant Raman process at the low temperature region in 2-4.

## Introduction

Single molecule magnets (SMMs) display slow magnetic relaxation and magnetic hysteresis arising from the electronic structure at molecular level and have attracted much attention due to the forward-looking applications such as quantum computing, spintronic devices, and high density data storage. Single ion magnets (SIMs), which contain a unique paramagnetic center, form an important subclass of SMMs. The extensive researches have been conducted to understand the origin and mechanism of slow magnetic relaxation and improve the performance of SIMs. Besides the extensively studied lanthanide-based SIMs, many transition-metal SIMs with various coordination numbers have been reported since the discovery of the first 3d-ion SIM based on mononuclear trigonal pyramidal Fe(II) complex in 2010 by Long and co-workers.

The Co(II) ion has been frequently used to construct molecule-based magnets because of its strong magnetic anisotropy. Moreover, Co(II) complexes have a high accessibility to model the magnetic behavior through tuning the coordination number,

geometry and electronic structure. To date, a variety of different coordination geometries of Co(II)-based SIMs including linear<sup>11</sup>, trigonal,<sup>12</sup> tetrahedral,<sup>13</sup> square-pyramidal,<sup>14</sup> distorted octahedral<sup>15</sup> pentagonal bipyramid,<sup>16</sup> and square antiprism<sup>17</sup> have been designed to attain strong magnetic anisotropy. Besides the coordination geometry, the nature of donor atoms has also been used to tune the magnetic anisotropy. In this regard, several studies have showed that heavier donor atoms like S, Se, Te, P and As would give larger and negative anisotropy in metal complexes.<sup>18</sup>

Recently, our group has reported two five-coordinate cobalt(II) complexes  $[Co(12\text{-TMC})(CH_3CN)](X)_2$   $(12\text{-TMC} = 1,4,7,10\text{-tetramethyl-1,4,7,10-tetraazacyclododecane, } X = BF_4^-, PF_6^-)$ , which are the first examples of the coexistence of field induced slow magnetic relaxation and spin-crossover. With the neutral tetradentate macrocyclic ligand 12-TMC to support the Co(II) center, the methyl group linked to N donor atoms would compel the Co(II) center out of the macrocyclic plane and leave one or two vacant sites accessible for further coordination. The metal coordination environment can thus be modified through simply using the different co-ligand to occupy the vacant coordinate sites. The co-ligands are expected to finely tune the magnetic anisotropy.

Herein we present the synthesis and magnetic properties of three mononuclear six-coordinate Co(II) complexes  $[Co(12TMC)X_2]$  with different pseudohalides,  $NCS^-(1)$ ,  $NCSe^-(2)$  and  $N(CN)_2^-(3)$ , and a five-coordinate complex  $[Co(12TMC)(NCO)][B(C_6H_5)_4]$  (4). The easy-plane magnetic anisotropy has been confirmed for the six-coordinate complexes 1-3 by magnetometry and high–frequency and –field EPR (HFEPR) spectroscopy. In contrast, the easy-axis anisotropy was found for 4. The ac susceptibility measurements demonstrate that they exhibit slow magnetic relaxation under an applied direct-current (dc) field. Remarkably, there are two relaxation processes observed in 1 and 2, which could be caused by

a. State Key Laboratory of Coordination Chemistry, School of Chemistry and Chemical Engineering, Nanjing University, Nanjing 210023, China. E-mail: xtchen@niu.edu.cn

b. Jiangsu Key Laboratory for NSLSCS, School of Physical Science and Technology, Nanjing Normal University, Nanjing 210023, China

Wuhan National High Magnetic Field Center, Huazhong University of Science and Technology, Wuhan 430074, China

d. Department of Chemistry, University of Tennessee, Knoxville, Tennessee 37996, USA.

<sup>†</sup>Electronic supplementary information (ESI) available: Figures of XRD patterns for 1-4; Table for the calculations by SHAPE; Table for the fitting data for the Cole-Cole plot; Additional figures for magnetic characterization and HFEPR data; Additional structural data in CIF format (CIF).See DOI: 10.1039/x0xx00000x

two molecules in the asymmetric unit. The detail of the relaxation dynamics of magnetization are reported as follows.

## **Experimental**

#### Materials and methods

All the solvents were dried and purified using conventional methods before use. The other chemicals employed were commercially available and used as received. 1, 4, 7, 10-Tetramethyl-1, 4, 7, 10-tetraazacyclododecane (12-TMC) was synthesized according to literature procedure. The synthetic experiments were carried out under N2 atmosphere with standard Schlenk techniques. Elemental analyses of C, H and N were performed on an Elementar Vario ELIII elemental analyzer. Powder X-ray diffraction (PXRD) patterns were measured on a Bruker D8 ADVANCE X-ray powder diffractometer with a Cu K $\alpha$  X-ray source ( $\lambda$  =1.54056 Å) at 40 kV and 40 mA. The phase purities of the complexes were confirmed with good agreement between the measured X-ray diffraction patterns and the simulated ones (Fig. S1-S4, ESI†). High-frequency and –field EPR (HFEPR) experiments were performed using a spectrometer constructed at the National High Magnetic Field Laboratory, USA. In the commercial spectrometer constructed at the National High Magnetic Field Laboratory, USA. In the commercial spectrometer constructed at the National High Magnetic Field Laboratory, USA.

#### Synthesis of complexes 1-4

[Co(12-TMC)(NCS)<sub>2</sub>]-0.5CH<sub>3</sub>OH (1). Co(NCS)<sub>2</sub> (0.5 mmol, 0.095 g) and 12-TMC (0.5 mmol, 0.09 g) were dissolved in 15 mL of CH<sub>3</sub>OH and stirred for 5 h at room temperature. A purple solution was formed and then filtrated. The purple crystals of 1 were obtained after several days by the diffusion of diethyl ether into the filtrate, with a yield of 70 % based on Co. Anal. Calc. for  $C_{29}H_{60}Co_2N_{12}OS_4$ : C, 41.52; H, 7.21; N, 20.03. Found: C, 41.58; H, 7.20; N, 20.10.

**[Co(12-TMC)(NCSe)<sub>2</sub>]·0.5CH<sub>3</sub>CN (2).** CoCl<sub>2</sub> (0.5 mmol, 0.065 g) and 12-TMC (0.5 mmol, 0.09 g) were dissolved in 15 mL of  $C_2H_5OH$  and stirred for 30 min at room temperature. KNCSe (1.0 mmol, 0.15 g) was added to the solution and stirred for another 5 h. The mixture was filtrated, and the precipitate was dissolved successively in acetonitrile. The purple crystals of **2** formed over several days by the diffusion of diethyl ether into the  $CH_3CN$  solution with a yield of 65% based on Co. Anal. Calc. for  $C_{30}H_{59}Co_2N_{13}Se_4$ : C, 34.79; H, 5.74; N, 17.58. Found: C, 34.75; H, 5.71; N, 17.60.

**[Co(12-TMC)(N(CN)**<sub>2</sub>)<sub>2</sub>**] (3). 3** was obtained according to the same procedure as **2**, but using 12-TMC (1.0 mmol, 0.18 g) and NaN(CN)<sub>2</sub> (1.0 mmol, 0.089 g) instead of 12-TMC (0.5 mmol, 0.09 g) KNCSe (1.0 mmol, 0.15g). The red crystals of **3** were obtained in 70% yield based on Co. Anal. Calc. for  $C_{16}H_{28}CoN_{10}$ : C, 45.82; H, 6.73; N, 33.40. Found: C, 45.80; H, 6.71; N, 33.43.

[Co(12-TMC)(NCO)][B( $C_6H_5$ )4] (4). CoCl<sub>2</sub> (0.5 mmol, 0.065 g) and 12-TMC (1.0 mmol, 0.18 g) were dissolved in 15 mL of  $C_2H_5OH$  and stirred for 30 min at room temperature. KNCO (0.5 mmol, 0.04 g) and Na[B( $C_6H_5$ )4] (0.5 mmol, 0.17 g) was added to the solution and stirred for another 5 h. The resulting blue precipitate was collected and then dissolved in 15 mL acetonitrile. The blue crystals of 4

formed over several days by the diffusion of diethyl ether into the solution with a yield of 71% based on Co. Anal. Calc. for  $C_{37}H_{48}BCoN_5O$ : C, 68.52; H, 7.46; N, 10.80. Found: C, 68.49; H, 7.45; N, 10.81.

#### X-ray single-crystal structure determination

Single-crystal X-ray diffraction data were collected on a Bruker APEX DUO diffractometer at 155 K with a CCD area detector (Mo K $\alpha$  radiation,  $\lambda$  = 0.71073 Å).  $^{22}$  The frames of data and unit cell parameters were determined using the APEX II program. The data was integrated by SAINT and corrected for Lorentz and polarization effects. Absorption corrections were applied using the multiscan program SADABS.  $^{23}$  The molecular structures were determined via full-matrix least-squares procedure SHELXL (version 2014/7).  $^{24}$  The hydrogen bonded to carbon were generated theoretically with isotropic thermal parameters riding on their parents. All non-hydrogen atoms were refined through full-matrix least-squares routine. A summary of the crystallographic data and refinement parameters are listed in Table S1.†

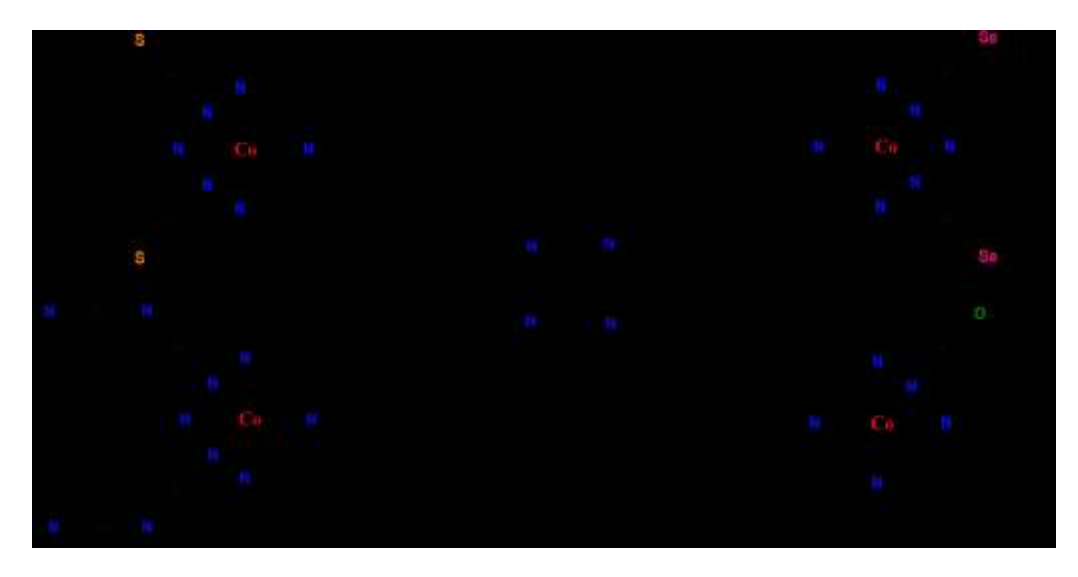
#### Magnetic measurements

Magnetic characterizations were carried out on a vibrating sample magnetometer (VSM) of Quantum Design MPMS SQUID-VSM system for ground microcrystalline powder of **1-4** restrained with eicosane within a polycarbonate plastic capsule in order to prevent solvent molecules from disappearance or any torquing caused by magnetic field. Direct-current (dc) magnetic data were collected in fields between 0 and 7 T at a temperature between 2 K and 300 K. Alternating-current (ac) susceptibility measurements were performed with an ac field of 0.2 mT at frequencies varying over the range of 1 to 999 Hz under different external fields. All experimental susceptibilities data were corrected for the diamagnetic contributions using Pascal's constants, included the sample holder as well as the diamagnetism of the sample.<sup>25</sup>

## **Results and discussion**

#### **Synthesis**

Initially we employed the reactions between  $Co^{2+}$  and 12TMC to synthesize the six-coordinate [(12-TMC)CoX<sub>2</sub>], with the different pseudohalides (NCS<sup>-</sup>, NCSe<sup>-</sup>, NCO and N(CN)<sub>2</sub><sup>-</sup>). The six-coordinated complexes **1-3** were expectedly obtained with X = NCS<sup>-</sup>, NCSe<sup>-</sup> and N(CN)<sub>2</sub><sup>-</sup>, while with NCO<sup>-</sup>, only five-coordinated complex [Co(12-TMC)(NCO)][B(C<sub>6</sub>H<sub>5</sub>)<sub>4</sub>] (**4**) was formed (Scheme 1). We have tried to use excess NCO<sup>-</sup> salt to prepare the six-coordinate analogue, but only five-coordinate complex **4** was formed. Such unusualness was only rarely observed. Khan et. al. observed the different coordination modes between the dinuclear copper(II) complexes with NCO<sup>-</sup> and NCS<sup>-</sup>.<sup>26</sup>



Scheme 1. Synthetic routes to complexes 1-4.

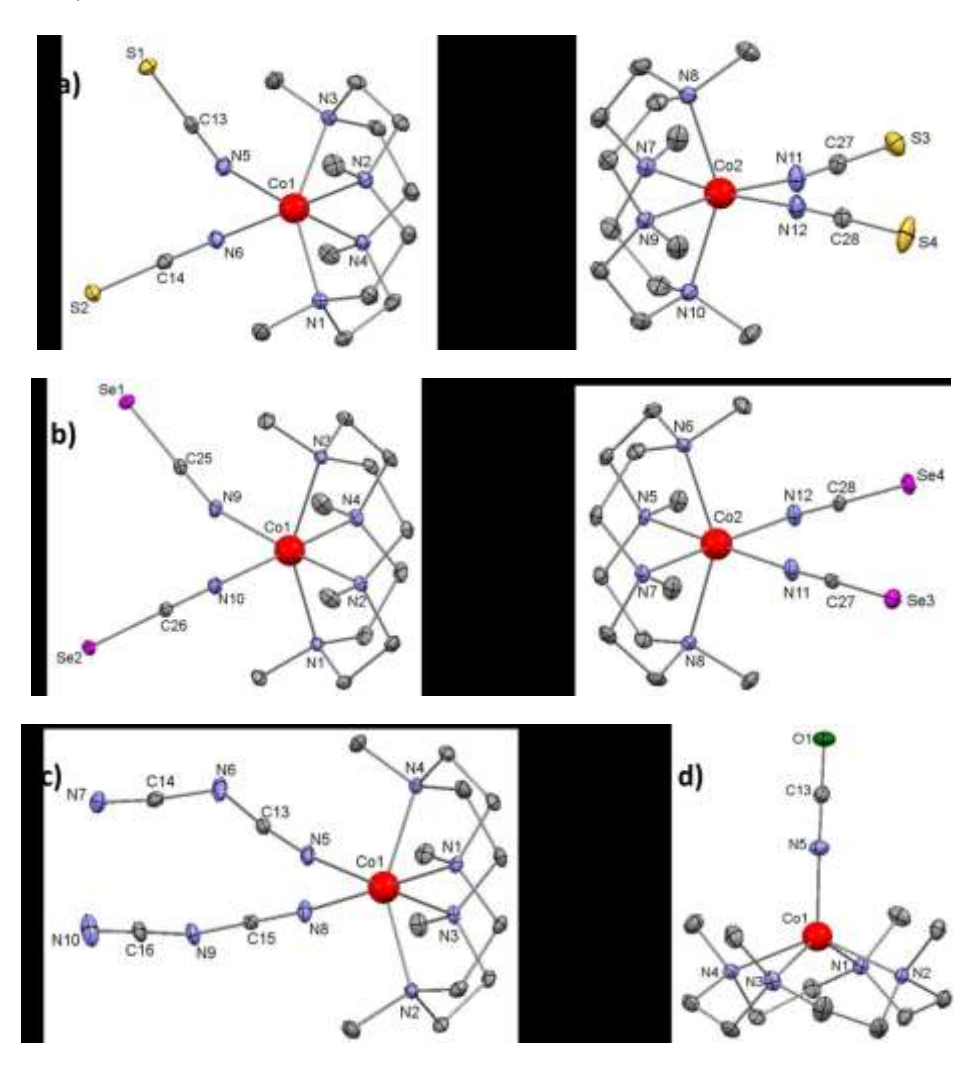


Fig. 1 (a) The octahedral Co<sup>II</sup> ion of two different molecules in the asymmetric unit of 1; (b) The two octahedral Co<sup>II</sup> ion of two different molecules in the asymmetric unit of 2; (c)
The octahedral Co<sup>II</sup> ion in 3; (d) The spherical square pyramidal Co<sup>II</sup> ion in 4. Red, blue, and gray spheres represent Co, N, and C atoms, and yellow, purple and green ones represent S, Se and O, respectively. All H atoms and solvent water molecules were omitted for clarity.

#### Structural descriptions

Complexes 1, 2 and 3 crystallize in the monoclinic space group  $P 2_1/n$ . The selected bond lengths and bond angles are afforded in Table 1. In contrast with only one unique molecule in 3 and 4, the asymmetric unit of complexes 1 and 2 consist of two crystallographically distinct molecules, which are labelled as 1a, 1b and 2a, 2b (Fig. 1), whose structural parameters vary slightly. The central Co<sup>II</sup> ions of these six-coordinate complexes are coordinated by six nitrogen atoms and adopt the distorted octahedral geometry. The two N atoms of pseudohalogen ions (NCS, 1; NCSe, 2; NCNCN, 3) in cis positions and two tertiary amine N atoms from the neutral tetradentate macrocyclic ligand 12TMC define the equatorial plane while the remaining two tertiary nitrogen atoms occupy the axial positions (Fig. 1a, 1b and 1c). In the equatorial positions, Co-N<sub>pseudohalide</sub> bonds in a range of 2.065(3)-2.1058(14) Å are shorter than the bond distances between Co<sup>II</sup> ion and the two N atoms of 12TMC ligand (2.252(3)-2.2826(13) Å), which are in turn larger than the Co-N<sub>12TMC</sub> bond distances in the axial positions (2.161(3)-2.195(3) Å). The equatorial N-Co-N bond angle involving the two cis- pseudohalide groups (83.38(6)-86.33(12)°) are smaller than that involving the two cis- nitrogen atoms of 12TMC ligand (100.99(9)-102.29(5)°). It can be seen that all of the angles in the equatorial plane deviate from the angle for an ideal octahedron with 90°. These angle distortions give a trapezoid in the equatorial plane. Furthermore, the axial bond angles between Co<sup>II</sup> ion and the N atoms of 12TMC ligand are more bent with a range of 146.76(10)-147.80(10)° compared with the bond angle for an ideal octahedron (180°). Such tilting of two axial ligands combining with the distortion of the equatorial base leads to a skew-trapezoidal bipyramid configuration for 1-3.27

In addition, a geometrical analysis was performed with the SHAPE program, <sup>28</sup> which is used to evaluate the degree of deviation from the ideal symmetry. The continuous shape measures (*CShMs*) of the Co<sup>II</sup> centers show that the distortion value is 3.277, 3.230 and 2.967 for **1**, **2** and **3**, respectively, indicating that their molecular geometries are distorted octahedron (Table S2, ESI†). Besides, there is no intermolecular interaction, such as hydrogen bonds, except for van der Waals' forces in the crystal lattice. The average shortest intermolecular Co---Co distances are 7.905 Å for **1**, 7.987 Å for **2** and 8.055 Å for **3**, respectively.

It is noted that the similar coordination geometry of two molecules in complexes  ${\bf 1}$  and  ${\bf 2}$ , but the most obvious difference is the bond angles between Co<sup>II</sup> ion and the pseudohalogen ions. For  ${\bf 1}$ , the two Co–N<sub>NCS</sub>–C<sub>NCS</sub> bond angles are rather bent with 149.3(3)° and 155.5(3)° in  ${\bf 1a}$  while those are identical with 173.4(4)° in  ${\bf 1b}$ . The corresponding Co–N–C bond angles are 153.2°and 155.4° in  ${\bf 2a}$ , 175.3°and 175.1° in  ${\bf 2b}$  and 163.20(15)° and 160.01(14)° in  ${\bf 3}$ . In addition, the two sets of N(CN)<sub>2</sub>- of complex  ${\bf 3}$  bent in the opposite direction, wherein the bond angles of C-N-C are 119.12° and 123.64°, respectively.

Complex 4 crystallizes in the monoclinic space group P  $2_1/c$ . It is five-coordinated with Co(II) center residing in the distorted square pyramidal configuration, consisting of four N atoms from 12-TMC ligand in equatorial basal plane and one N atom from the NCO-group in the apical position (Fig. 1d). The Co(II) center lies out of the basal plane by 0.802 Å. The average Co–Nequatorial bond distance is 2.161 Å, which is longer than the bond distances of Co–N<sub>NCO</sub> with

1.9399(17) Å. The greater basal angles of N-Co-N are almost equal with 136.0(2)° and 136.71(13)°, which is comparable to the structure as a perfectly square pyramidal with  $C_{4\nu}$  geometry. The shortest intermolecular Co---Co distances is 7.094 Å in **4**. Moreover, the continuous shape measures (*CShMs*) of the Co<sup>II</sup> center were calculated by SHAPE software. The distortion value is 0.442 (Table S2, ESI†), which is close to zero for an ideal square pyramidal geometry.

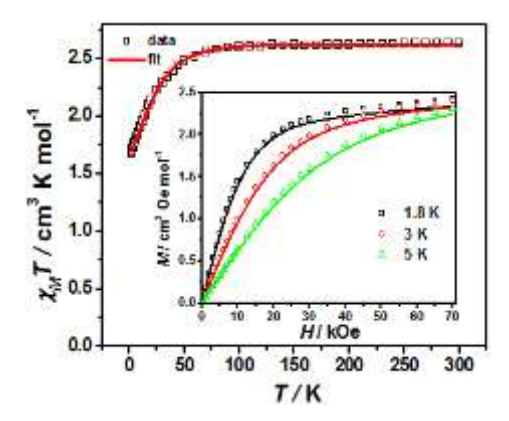
Table 1. Selected Bond Lengths (Å) and Angles (deg) for complexes 1-4.

Table 1. Selected Bond Lengths (A) and Angles (deg) for complexes 1-4.							
1a			1b				
Co1-N1	2.190(3)	Co2-N7	2.304(3)				
Co1-N2	2.294(3)	Co2-N8	2.180(3)				
Co1-N3	2.193(2)	Co2-N9	2.316(2)				
Co1-N4	2.264(3)	Co2-N10	2.180(3)				
Co1-N5	2.065(3)	Co2-N11	2.073(3)				
Co1-N6	2.080(3)	Co2-N12	2.072(3)				
N1-Co1-N3	146.78(9)	N8-Co2-N10	146.76(10)				
N2-Co1-N4	101.60(9)	N7-Co2-N9	100.99(9)				
N5-Co1-N6	84.28(11)	N11-Co2-N12	86.33(12)				
N2-Co1-N5	86.09(10)	N7-Co2-N11	86.19(10)				
N4-Co1-N6	89.30(10)	N9-Co2-N12	86.82(11)				
C13-N5-Co1	155.5(3)	C27-N11-Co2	173.4(3)				
C14-N6-Co1	149.3(3)	C28-N12-Co2	173.4(3)				
	2a		2b				
Co1-N1	2.195(3)	Co2-N5	2.304(2)				
Co1-N2	2.252(3)	Co2-N6	2.174(3)				
Co1-N3	2.192(3)	Co2-N7	2.307(3)				
Co1-N4	2.276(3)	Co2-N8	2.161(3)				
Co1-N9	2.073(3)	Co2-N11	2.081(3)				
Co1-N10	2.080(3)	Co2-N12	2.083(3)				
N1-Co1-N3	147.80(10)	N6-Co2-N8	147.67(10)				
N2-Co1-N4	101.90(10)	N5-Co2-N7	101.54(9)				
N9-Co1-N10	83.85(11)	N11-Co2-N12	85.88(11)				
N2-Co1-N10	89.14(10)	N5-Co2-N12	86.85(10)				
N4-Co1-N9	86.42(10)	N7-Co2-N11	85.83(10)				
C25-N9-Co1	153.2(3)	C27-N11-Co2	175.1(3)				
C26-N10-Co1	155.4(3)	C28-N12-Co2	175.3(3)				
	3		4				
Co1-N1	2.2731(13)	Co1-N1	2.108(3)				
Co1-N2	2.1762(14)	Co1-N2	2.161(4)				
Co1-N3	2.2826(13)	Co1-N3	2.169(7)				
Co1-N4	2.1791(14)	Co1-N4	2.205(3)				
Co1-N5	2.1058(14)	Co1-N5	1.9399(17)				
Co1-N8	2.0756(15)	N1-Co1-N2	82.33(10)				
N2-Co1-N4	147.78(5)	N1-Co1-N4	82.68(10)				
N1-Co1-N3	102.29(5)	N2-Co1-N3	82.48(14)				
N5-Co1-N8	83.38(6)	N1-Co1-N3	136.0(2)				
N1-Co1-N5	86.75(5)	N2-Co1-N4	136.71(13)				
N3-Co1-N8	88.03(5)	N3-Co1-N4	80.88(14)				
C13-N5-Co1	163.20(15)	N1-Co1-N5	117.12(10)				
C15-N8-Co1	160.01(14)	N2-Co1-N5	106.84(11)				
C14-N6-C13	123.64(17)	N3-Co1-N5	106.70(2)				
C16-N9-C15	119.12(15)	N4-Co1-N5	116.16(10)				

## Static magnetic properties and HF-EPR spectra

The direct-current (dc) magnetic susceptibilities were measured on polycrystalline samples of **1-4** under a dc field of 0.1 T in the 2–300 K temperature range. The obtained temperature dependence of  $\chi_M T$  products are shown in Fig. 2 and S5-S7†. The room temperature  $\chi_M T$  values are 2.66, 2.65, 2.61 and 3.01 cm³ K mol<sup>-1</sup> for **1-4**, respectively, which are higher than the theoretical spin-only value of 1.875 cm³ K mol<sup>-1</sup> for the mononuclear high-spin Co(II) center (S = 3/2, g = 2.0). They are in the reported range of 2.1–3.4 cm³ K mol<sup>-1</sup> for anisotropic high-spin Co(II) center, <sup>29</sup> which are ascribed to the significant orbital contribution. Upon cooling from room temperature, the  $\chi_M T$  product remains constant until 80-90 K for **1-4**, and then slightly decreases to 1.68, 1.66, 1.65 and 1.97 cm³ K mol<sup>-1</sup>, respectively, at 2 K. The downturn of  $\chi_M T$  value at low

temperature is due to the inherent magnetic anisotropy of the Co<sup>II</sup> ion rather than the intermolecular antiferromagnetic interactions between the metal ions considering the large intermolecular Co--- Co separations.



**Fig. 2** Variable-temperature dc susceptibility data of **1** under applied dc field of 0.1 T Inset: field-dependent the magnetizations below 5 K. Solid lines are fits to the data with program  $PHI^{31}$ .

Furthermore, the field-dependent magnetisations were determined for **1-4** at applied magnetic fields ranging from 0 to 7 T at 1.8, 3.0 and 5.0 K, respectively (inset, Fig. 2, and S6-S7, ESI+). The magnetisation data attain the values of 2.42, 2.43, 2.47 and 2.44  $N_A\mu_B$  at 7 T and 1.8 K for **1-4**, respectively, which are far lower than the theoretical saturation value of 3  $N_A\mu_B$  for an isolated Co<sup>II</sup> ion (g = 2, S = 3/2), indicating the magnetizations do not achieve saturation at 7 T.

To analyse the magnitude and nature of the magnetic anisotropy, we employ the full Hamiltonian as given in eqn (1), which considers the strong orbital contribution to the magnetic moment for the Co(II) complexes where the unquenched orbital moment contribute strongly to the magnetic moment.

$$\hat{H} = \sigma \lambda \hat{L} \cdot \hat{S} + \sigma^2 (B_2^0 (3\hat{L}_z^2 - \hat{L}^2) + \frac{B_2^2}{2} (\hat{L}_+^2 + \hat{L}_-^2)) + \mu_B (\sigma \hat{L} + 2\hat{S}) \cdot H$$
 (1) \_

where  $\sigma$  represents a combined orbital reduction parameter  $\sigma = -A \cdot \kappa$ . The A parameter is required when using the T=P equivalence for orbital triplet terms and takes the value of 1.0 when representing a T<sub>2</sub> term and 3/2 when representing a T<sub>1</sub> term. The  $\kappa$  parameter considers the reduction of the orbital momentum caused by the delocalization of the unpaired electrons.  $\lambda$ ,  $B_2^o$  and  $B_2^o$  represent the spin-orbit coupling constant and crystal field parameters (CFPs)<sup>30</sup>. The fit to the dc magnetic susceptibilities of six-coordinate complexes 1-3 using  $PHI^{31}$  program gives the reasonable parameters, which were listed in Table 2. The fitting curves match well with the experimental data in the range of whole temperature (Fig. S5, ESI†). From the fitting results of the magnetic susceptibilities above, it can be concluded that the parameters  $B_2^o$  are positive, representing the easy-plane magnetic anisotropies, which are consistent with the following HFEPR data.

When the  $B_2^0$  parameter is positive and relatively large,  ${}^4A_{2g}$  can be considered as the ground term, which is well-separated from the excited term  ${}^4E_g$ . Then, the energy gap between the two Kramers doublets of  $M_S = \pm 1/2$  and  $M_S = \pm 3/2$  splitting from the  ${}^4A_{2g}$  term can be associated with an axial ZFS.  ${}^{15a,15b}$  In this case, the magnetic

properties may be interpreted with the spin Hamiltonian as shown in eqn. (2):

$$H = D(\hat{S}_{z}^{2} - S(S+1)/3) + E(\hat{S}_{y}^{2} - \hat{S}_{y}^{2}) + \mu_{R}g\hat{S} \cdot H$$
 (2)

where D, E, S, H, and  $\mu_B$  represent the axial and rhombic ZFS parameters, the spin operator, magnetic field vectors, and the Bohr magneton, respectively. To estimate the zero-field splitting parameters D and E of the Co(II) centres in **1-3**, the experimental susceptibility and magnetization data were fitted simultaneously using the program PHI. The best-fit values of the parameters were showed in Table 2 for **1-3**. As we can see, the signs of ZFS parameters D are determined to be positive with the values of 32.10, 33.49, and 25.95 for **1-3**, respectively. These values show significant easy-plane anisotropies of the Co(II) centre in **1-3**.

For the five-coordinate complex **4** with a square-pyramid configuration, the orbital moment could contribute greatly to the magnetic properties.  $^{14d,14e}$  The magnetic susceptibility data of **4** was also modelled with the general Hamiltanian as shown in eqn (1) by the program  $PHI^{31}$ . It was found that no unique set of fitting parameters were obtained. To avoid the overparameterisation, we fix the rhombic crystal parameter  $B_2^2$  as zero and treat magnetic data with three parameters  $\sigma$ ,  $\lambda$ , and  $B_2^o$ . The fitting parameters are listed in Table 2. The negative value of  $B_2^o$  shows the easy axis magnetic anisotropy of **4**, which is in agreement with the HFEPR spectra.

Table 2. The fitting parameters obtained experimentally for complexes 1-4.

	1	2	3	4	
fittings of the dc magnetic					
data with eqn (1) by PHI.31					
Orbital reduction factor $\sigma$	-1.17	-1.16	-1.18	-1.35	
$\lambda$ , cm <sup>-1</sup>	-82.66	-88.72	-73.83	-88.17	
$B_2^0$ , cm <sup>-1</sup>	98.85	102.23	95.61	-89.82	
$B_2^2$ , cm <sup>-1</sup>	96.94	89.91	85.94	/	
fittings of the dc magnetic					
data with eqn (2) by PHI.31					
<i>D</i> , cm <sup>-1</sup>	32.10	33.49	25.95	/	
<i>E</i> , cm <sup>-1</sup>	0.32	0.16	0.12	/	
$g_{x,y}$	2.46	2.44	2.43	/	
$g_z$	2.13	2.20	2.16	/	

To confirm the nature of the magnetic anisotropies in 1-4, highfield and -frequency electron paramagnetic resonance (HFEPR) spectra<sup>32</sup> were recorded for the powder samples of 1-4 at different frequencies (Fig. 3 and S8-S11, ESI+). For complex 3, the spectrum at the frequency of 100 GHz at 4.2 K shows the three features with  $g_x = 5.90$ ,  $g_y = 3.89$ , and  $g_z = 1.81$ . This pattern of g values  $(g_x, g_y > g_z)$ is typical for a spin 3/2 system with large and positive D values. 15a,33 All features were from the intra-Kramers transitions within the lowest doublet  $M_S = \pm 1/2$  with  $\Delta M_S = \pm 1$ . A 2D resonating field versus frequency map was derived from the observed features (Fig. 3), indicating that these spectra can be interpreted in terms of an effective  $S_{eff}$  = 1/2 state and effective g values, which were also modeled with the spin-Hamiltanian.<sup>34</sup> It can be concluded that the simulated spectrum is more reasonable when the D value is positive with  $+ 25 \text{ cm}^{-1}$  and  $E = 6.5 \text{ cm}^{-1}$  instead of negative. For complexes 1-2, there are two sets of three EPR features observed, which are in accord with two crystallographically different molecules in the crystal lattices (Fig. S8-S9, ESI†). The patterns of g values ( $g_x$ ,  $g_y > g_z$ ) are also in agreement with the large and positive D values. 15a,33



**Fig. 3** Left: The experimental and simulation spectra for complex **3** under 100 GHz in derivative mode at 4.2 K. Right: Frequency dependence of the high-frequency EPR peak positions deduced from studies of powder samples of **3** at 4.2 K. The squares are the experimental points while green, blue, and red curves are generated by fitting using program *SPIN*<sup>34</sup> with the magnetic field parallel to the x, y, and z axes of the ZFS tensor, respectively.

The HFEPR spectra for the powdered sample of **4** at 4.2 K and 112 GHz (Fig. S10, ESI†) shows only a single parallel-type transition occurring at an effective g value of  $g^{eff}$  =7.01(4). There is only one strong signal observed at  $g^{eff} \approx 7$ , confirming the easy axis type anisotropy for Co(II) center.<sup>13d</sup> These observations are in agreement with the results obtained by fitting the magnetic data of **4**.

#### Theoretical studies of magnetic anistropy in 1-4

In order to get further insight into the nature of magnetic anisotropies of **1-4**, theoretical studies were performed on **1-4** by the complete active space second-order multiconfigurational perturbation theory (CASPT2) considering the effect of the dynamic electron correlation based on complete-active-space self-consistent field (CASSCF) method with MOLCAS 8.2 program package. Calculation details are given in ESI<sup>†</sup>.

The energies of the spin-free states and spin-orbit states were calculated, which are listed in Tables S3-S4<sup>†</sup>. The first excited spinfree state is in the range of 1440.1-1687.2 cm<sup>-1</sup> above the ground one for 1-3, which means that the lowest quartet term is well isolated from the excited ones for 1-3. These energy differences between the lowest two spin-free states are much larger than those between the lowest two spin-orbit states. Furthermore, the spinorbit ground states are mainly composed from the ground one. The orbital nondegeneracy of the ground term allow us to use spin Hamiltanian as shown in eqn (2) with the ZFS parameters D and E to model their magnetic anisotropies. The calculated D, E (cm $^{-1}$ ) and gtensor (x, y, z) of **1–3** are listed in Table S5<sup>†</sup>. The calculated D values are +26.6, +24.5, +27.4, +25.9 and +22.5 cm<sup>-1</sup> for 1a, 1b, 2a, 2b and 3, respectively, which are comparable to those derived from the magnetic data. The calculated g values are consistent with the easyplane anisotropies in **1-3**. The calculated  $\chi_M T$  versus T and M versus H plots of 1-3 are shown in Fig. S12-S13<sup>†</sup>. The calculated orientations of the local main magnetic axes on Co<sup>II</sup> ion of **1-3** are shown in Fig. S14<sup>†</sup>.

For complex 4, the energy gap (375.7 cm $^{-1}$ ) between the lowest two spin-free states is in agreement with the quasi-degeneracy related to the  $^4$ E term in the idealized  $C_{4v}$  symmetry.  $^{14d,14e}$  This energy gap is larger than that between the

lowest two spin-orbit states (162.3 cm<sup>-1</sup>). However, the spin-orbit ground state is composed from the lowest two spin-free states, not just from the ground one (Table S4, ESI†). These suggest that there is very strong first-order spin-orbital coupling in **4** and zero-field splitting parameters D and E cannot be used to depict its magnetic anisotropy. Therefore the traditional spin Hamiltanian can not be used to model the magnetic data and HFEPR spectra.  $^{14d,14e}$  The calculated S=1/2 effective g-values of the ground state Kramers doublet of the Co<sup>II</sup> centre of **4** are  $g_x=0.541$ ,  $g_y=0.735$ , and  $g_z=9.253$  (Table S6, ESI†), demonstrating its easy-axis anisotropy. The magnetic susceptibilities and magnetizations of **4** were also calculated as shown in Fig. S12-S13†, which are comparable to the experimental curves. Furthermore, the calculated orientations of the  $g_x$ ,  $g_y$ ,  $g_z$  (easy axis) of the ground doublet on the Co<sup>II</sup> ion was shown in Fig. S14†.

#### **Dynamic magnetic properties**

To investigate the relaxation dynamics of **1–4**, alternating-current (ac) susceptibility measurements were carried out in the temperature range of 1.8–6 K with an alternating field of 0.2 mT oscillating with 1–999 Hz under different dc fields (Fig. 4 and S15-S26, ESI†). Unfortunately, no out-of-phase ( $\chi_M$ ") signals were detected under zero applied dc field. However, all complexes exhibit strong frequency-dependent ac susceptibilities under a small external dc field. The absence of out-of-phase ( $\chi_M$ ") signals under zero applied field could be caused by the occurrence of strong quantum tunneling of magnetization (QTM), which has been observed in most Co(II)-based SIMs.  $^{11-17}$ 

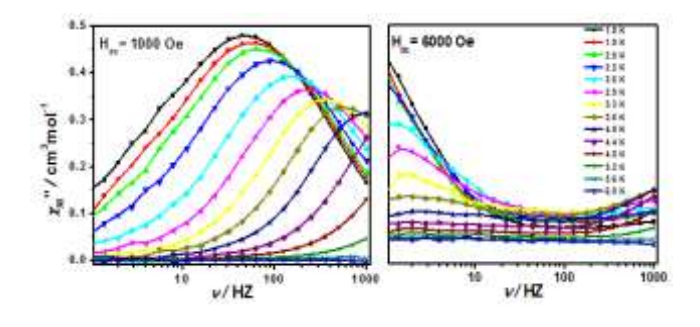


Fig. 4 Frequency dependence of the ac susceptibility from 1.8 to 6 K for  $\bf 1$  under 0.1 T (left) and 0.6 T (right). The solid lines are for eye guide.

For **1** and **2**, there is only one magnetic relaxation process under an external dc field from 0.02 to 0.1 T. However, two slow relaxations were observed in the  $\chi_{M}$ " vs v plot with the increase of the external dc field until 0.6 T, which could be in consistent with the two crystalliographically different molecules in the crystal lattice. Hence, 0.1 T and 0.6 T were chosen for **1** and 0.08 T and 0.6 T for **2** to perform further ac magnetic measurements in the temperature range of 1.8-6.0 K (Fig. 4 and S16-S22, ESI†). Under these two different external dc fields, only one slow magnetic relaxation was observed in the whole temperature range. The plot of  $ln(\tau)$  versus  $T^{-1}$  were extracted from the peak value of the variable-frequency susceptibility data under 0.1 T, which were fitted with Arrhenius' law  $\tau = \tau^0 exp(U_{eff}/k_BT)$ , giving the effective energy barrier with the preexponential factor as  $U_{eff} = 8.2 \text{ cm}^{-1}$  ( $\tau_0 = 1.1 \times 10^{-5} \text{ s}$ ) for **1**,  $U_{eff} = 10.4 \text{ cm}^{-1}$  ( $\tau_0 = 3.0 \times 10^{-6} \text{ s}$ ) for **2**, respectively

(Fig. S23, ESI†). These derivations are based on the assumption that the thermally activated Orbach process is the dominant relaxation mechanism in the higher temperature range. The obtained  $\tau_0$  values are obviously too large for an Orbach process compared with those found in other Co(II) SIMs.  $^{11-17}$  Given the possible coexistence of multiple relaxations due to the curvature found in the Arrhenius plots, other mechanisms such as Raman process may occur in the magnetic relaxation of 1 and 2. On these grounds, we model the relaxation rates employing the Raman and Orbach relaxation processes by using eqn (3):  $^{35}$ 

$$\tau^{-1} = CT^n + \tau_0^{-1} \exp(-U_{eff} / kT)$$
 (3)

where the first term represents the contribution of the Raman or Raman-like process and the second term is for the Orbach process. The fitting curve with eqn (3) accords well with the data over the whole temperature range, with the following parameters: C = 46.38 S<sup>-1</sup>K<sup>-3</sup>, n = 3.2,  $\tau_0 = 5.2 \times 10^{-9}$  s,  $U_{eff} = 31.1$  cm<sup>-1</sup> for **1** and C = 127.4 S<sup>-1</sup>K<sup>-3</sup>, n = 2.3,  $\tau_0 = 6.4 \times 10^{-8}$  s,  $U_{eff} = 21.4$  cm<sup>-1</sup> for **2** (Fig. 5a and S24, ESI†). Therefore it can be concluded that the optical acoustic Raman-like mechanism is the dominant process in the studied temperature range in **1**. But in **2** the Raman process is dominated but the Orbach mechanism contributes to a less extent in high temperature range.

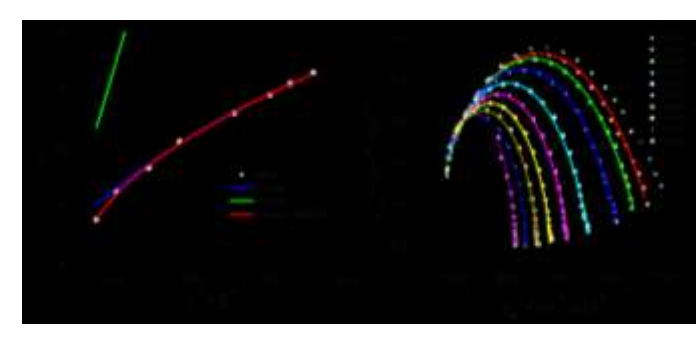


**Fig. 5** (a) Relaxation time of the magnetization  $In(\tau)$  vs  $T^1$  plots for **1**. (b) Cole-Cole plot obtained from the ac susceptibility data under different range of temperature for **1**. Solid lines represent the best fits to a generalized Debye model<sup>36</sup>.

Relaxation times under 0.6 T for 1-2 were extracted from the variable-temperature susceptibility data of high-frequency area. The  $In(\tau)$  vs  $T^{-1}$  plots were also fitted with Arrhenius' law  $\tau$  =  $\tau^0 exp(U_{eff}/k_BT)$  (Fig. S25, ESI†). We can derive the effective energy barrier with the preexponential factor as  $U_{eff}$  = 23.23 cm<sup>-1</sup> ( $\tau_0$  = 3.0 ×  $10^{-8}$  s) for **1**,  $U_{eff} = 25.53$  cm<sup>-1</sup> ( $\tau_0 = 1.8 \times 10^{-8}$  s) for **2**. Because the data were extracted from the peak value of the temperature dependence of out-of-phase ac susceptibility ( $\chi_M$ "), which were in the high-frequency and -temperature region, so it can be considered that the Orbach mechanism is the dominant process under 0.6 T. The Cole-Cole plots from the ac magnetic susceptibility data were also constructed (Fig. 5b and S26, ESI+) and fitted by the generalized Debye model<sup>36</sup> to give the isothermal susceptibility ( $\chi_{\tau}$ ), adiabatic susceptibility ( $\chi_s$ ),  $\tau$ , and  $\alpha$  parameters. The  $\alpha$  parameters are in a range of 0.10-0.41 for 1 and 0.08-0.33 for 2, suggesting the relatively narrow distribution of the relaxation time (Table S7, ESI†).

For investigation of the relaxation dynamics of **3** and **4**, 0.2 T and 0.1 T fields were chosen to perform additional ac measurements, respectively (Fig. S27-S30, ESI†). There is only one magnetic relaxation process under an external dc field. The plot of  $In(\tau)$  versus  $T^{-1}$  extracted from the variable-frequency susceptibility data

were fitted with eqn (3), giving the following parameters of C=2.4 S<sup>-1</sup>K<sup>-3</sup>, n=3.7,  $\tau_0=1.4\times10^{-8}$  s,  $U_{eff}=26.8$ cm<sup>-1</sup> for **3** and C=11.3 S<sup>-1</sup>K<sup>-3</sup>, n=4.8,  $\tau_0=1.4\times10^{-9}$  s,  $U_{eff}=22.7$  cm<sup>-1</sup> for **4** (Fig. S31, ESI<sup>+</sup>). It shows that the Raman process is the dominated mechanism at the low temperature region while the Orbach mechanism dominates at high temperature range for both **3** and **4**. The Cole–Cole plots (Fig. S32, ESI<sup>+</sup>) were also constructed by fitting of the  $\chi_M$ " versus  $\chi_M$  data by the generalized Debye model, <sup>36</sup> yielding the isothermal susceptibility ( $\chi_T$ ), adiabatic susceptibility ( $\chi_S$ ),  $\tau$ , and  $\alpha$  parameters, which are listed in Table S7<sup>+</sup>. The obtained  $\alpha$  parameters are in the range of 0.08-0.35 and 0.09-0.17 for **3** and **4**, respectively. Compared with six-coordinate Co(II) complexes **1**, **2** and **3**, the five-coordinate Co(II) complexes of **4** signifies a narrower relaxation distribution.

### **Conclusions**

In conclusion, this report presents the synthesis and characterization of four field-induced SIMs based on Co<sup>II</sup> ion supported by a macrocyclic ligand 12TMC and commitantly adjusted by the pseudohalogen ligands, namely, NCS- (1), NCSe<sup>-</sup> (2), N(CN)<sub>2</sub><sup>-</sup> (3) and NCO<sup>-</sup> (4). Different from sixcoordinate complexes 1, 2, and 3, complex 4 is fivecoordinated with NCO occupying at the axial position. It can be revealed that there are easy-plane anisotropies in all sixcoordinate complexes by direct magnetic measurements and HFEPR spectroscopy and theoretical studies, while it is easyaxis anisotropy in five- coordinate complex. The detailed study of the dynamic susceptibilities revealed that complexes 1 and 2 show two slow relaxation processes under an external dc field, consistent with two different molecules in the crystal lattice, which is rare in the previously reported transition metal ion SIMs.<sup>37</sup> The relaxation processes are taking place with Raman process being dominated at the low temperature region and the Orbach mechanism contributes to some extent at high temperature range. The present work shows the slight change in the magnetic anisotropy and the slow relaxation dynamics within SMMs by structural modification by the pseudohalides. We believe that our research will enrich and deepen the study on field-induced Co(II) SIMs.

## **Conflicts of interest**

There are no conflicts to declare.

## **Acknowledgements**

We are grateful for the financial support from the Natural Science Grant of China (No. 21471078 to XTC and and 11774178 to YQZ) and the US National Science Foundation (CHE-1362548 and CHE-1633870 to ZLX).

## **Notes and references**

1 (a) M. N. Leuenberger and D. Loss, *Nature*, 2001, **410**, 789–793; (b) M. Affronte, *J. Mater. Chem.*, 2009, **19**, 1731–1737;

This journal is © The Royal Society of Chemistry 20xx

J. Name., 2013, **00**, 1-3 | **7** 

- (c) F. Troiani and M. Affronte, Chem. Soc. Rev., 2011, 40, 3119–3129.
- (a) L. Bogani and W. Wernsdorfer, Nat. Mater., 2008, 7, 179–186;
   (b) M. Urdampilleta, S. Klyatskaya, J.-P. Cleuziou, M. Ruben and W. Wernsdorfer, Nat. Mater., 2011, 10, 502–506.
- 3 (a) W. Wernsdorfer, N. A. Alcalde, D. N. Hendrickson and G. Christou, *Nature*, 2002, 416, 406; (b) S. Thiele, F. Balestro, R. Ballou, S. Klyatskaya, M. Ruben and W. Wernsdorfer, *Science*, 2014, 344, 1135–1138.
- 4 (a) N. Ishikawa, M. Sugita, T. Ishikawa, S. Y. Koshihara and Y. Kaizu, J. Am. Chem. Soc., 2003, 125, 8694–8695; (b) J. D. Rinehart, M. Fang, W. J. Evans and J. R. Long, Nat. Chem., 2011, 3, 538–542; (c) D. N. Woodruff, R. E. P. Winpenny and R. A. Layfield, Chem. Rev., 2013, 113, 5110–5148; (d) H. L. C. Feltham and S. Brooker, Coord. Chem. Rev., 2014, 276, 1–33.
- (a) G. A. Craig and M. Murrie, Chem. Soc. Rev. 2015, 44, 2135-2147; (b) A. K. Bar, C. Pichon and J.-P. Sutter, Coord. Chem. Rev., 2016, 308, 346-380; (c) J. M. Frost, K. L. M. Harriman and M. Murugesu, Chem. Sci., 2016, 7, 2470-2491; (d) M. Feng and M. -L. Tong, Chem. Eur. J. 2018, 24, 7574–7594
- 6 Y. -F. Deng, T. Han, Z. X. Wang, Z. W. Ouyang, B. Yin, Z. P. Zheng, J. Krzystek and Y.-Z. Zheng, *Chem. Commun.*, 2015, 51, 17688–17691.
- (a) L. Chen, J. Wang, Y. -Z. Liu, Y. Song, X. -T. Chen, Y. -Q. Zhang and Z. -L. Xue, Eur. J. Inorg. Chem., 2015, 2, 271–278;
   (b) J. Vallejo, A. Pascual-Alvarez, J. Cano, I. Castro, M. Julve, F. Lloret, J. Krzystek, G. De Munno, D. Armentano, W. Wernsdorfer, R. Ruiz-Garcia and E. Pardo, Angew. Chem. Int. Ed., 2013, 52, 14075–14079;
   (c) M. Ding, G. E. Cutsail III, D. Aravena, M. Amoza, M. Rouzières, P. Dechambenoit, Y. Losovyj, M. Pink, E. Ruiz, R. Clèrac and J. M. Smith, Chem. Sci., 2016, 7, 6132-6140.
- (a) D. E. Freedman, W. H. Harman, T. D. Harris, G. J. Long, C. J. Chang and J. R. Long, J. Am. Chem. Soc., 2010, 132, 1224–1225;(b) J. M. Zadrozny, D. J. Xiao, M. Atanasov, G. J. Long, F. Grandjean, F. Neese and J. R. Long, Nat. Chem., 2013, 5, 577–581; (c) P. P. Samuel, K. C. Mondal, N. Amin Sk, H. W. Roesky, E. Carl, R. Neufeld, D. Stalke, S. Demeshko, F. Meyer, L. Ungur, L. F. Chibotaru, J. Christian, V. Ramachandran, J. van Tol and N. S. Dalal, J. Am. Chem. Soc., 2014, 136, 11964–11971.
- 9 (a) R. C. Poulten, M. J. Page, A. G. Algarra, J. J. Le Roy, I. López, E. Carter, A. Llobet, S. A. Macgregor, M. F. Mahon, D. M. Murphy, M. Murugesu and M. K. Whittlesey, J. Am. Chem. Soc., 2013, 135, 13640–13643; (b) K. E. R. Marriott, L. Bhaskaran, C. Wilson, M. Medarde, S. T. Ochsenbein, S. Hill and M. Murrie, Chem Sci., 2015, 6, 6823-6828.
- R. Boča, C. Rajnák, J. Titič and D. Valigura, *Inorg. Chem.*, 2017, **56**, 1478-1482.
- P. C. Bunting, M. Atanasov, E. Damgaard-M
  Øller, M. Perfetti,
   I. Crassee, M. Orlita, J. Overgaard, J. V. Slageren, F. Neese and J. R. Long, Science, 2018, 362.
- 12 (a) A. Eichhöfer, Y. Lan, V. Mereacre, T. Bodenstein and F. Weigend, *Inorg. Chem.*, 2014, **53**, 1962–1974; (b) F. Deng, T.Han, B. Yin and Y.-Z. Zheng, *Inorg. Chem. Front.*, 2017, 4, 1141–1148.
- 13 (a) J. M. Zadrozny and J. R. Long, J. Am. Chem. Soc., 2011, 133, 20732–20734; (b) J. M. Zadrozny, J. Liu, N. A. Piro, C. J. Chang, S. Hill and J. R. Long, Chem. Commun., 2012, 48, 3927–3929; (c) .Y. Rechkemmer, F. D. Breitgoff, M. van der Meer, M. Atanasov, M. Hakl, M. Orlita, P. Neugebauer, F. Neese, B. Sarkar and J. van Slageren, Nat. Commun., 2016, 7, 10467; (d) P. Cucos, F. Tuna, L. Sorace, I. Matei, C. Maxim, S. Shova, R. Gheorghe, A. Caneschi, M. Hillebrand and M. Andruh, Inorg. Chem., 2014, 53, 7738–7747.
- 14 (a) T. Jurca, A. Farghal, P.-H. Lin, I. Korobkov, M. Murugesu and D. S. Richeson, J. Am. Chem. Soc., 2011, 133, 15814-

- 15817; (b) C. Rajnák, J. Titiš, O. Fuhr, M. Ruben and R. Boča, *Inorg. Chem.*, 2014, **53**, 8200–8202; (c) A. K. Mondal, T. Goswami, A. Misra and S. Konar, *Inorg. Chem.*, 2017, **56**, 6870–6878; (d) C. Rajnák, F.Varga, J. Titiš, J. Moncoľ and R. Boča, *Eur. J. Inorg. Chem.* 2017, 1915–1922; (e) A. Świtlicka, B. Machura, M. Penkala, A. Bieńko, D. C. Bieńko, J. Titiš, C. Rajnák and R. Boča, *Inorg. Chem.*, 2018, 57, 12740–12755.
- 15 (a) J. Vallejo, I. Castro, R. Ruiz-García, J. Cano, M. Julve, F. Lloret, G. De Munno, W. Wernsdorfer and E. Pardo, J. Am. Chem. Soc., 2012, 134, 15704–15707; (b) A. V. Palii, D. V. Korchagin, E. A. Yureva, A. V. Akimov, E. Y. Misochko, G. V. Shilov, A. D. Talantsev, R. B. Morgunow, S. M. Aldoshin and B. S. Tsukerblat, Inorg. Chem., 2016, 55, 9696–9706. (c) R. Herchel, L. Váhovská, I. Potočňák and Z. Trávníček, Inorg. Chem., 2014, 53, 5896–5898; (d) V. Chandrasekhar, A. Dey, A. J. Mota and E. Colacio, Inorg. Chem., 2013, 52, 4554–4561;
- 16 (a) L. Chen, S.-Y. Chen, Y.-C. Sun, Y.-M. Guo, L. Yu, X.-T. Chen, Z.-X. Wang, Z. W. Ouyang, Y. Song and Z. -L. Xue, *Daton. Trans.*, 2015, **44**, 11482-11490; (b) X.-C. Huang, C. Zhou, D. Shao and X.-Y. Wang, *Inorg. Chem.*, 2014, **53**, 12671-12673.
- 17 L. Chen, J. Wang, J. -M. Wei, W. Wernsdorfer, X. -T. Chen, Y. -Q. Zhang, Y. Song and Z. -L. Xue, J. Am. Chem. Soc., 2014, 136, 12213–12216.
- (a) J. M. Zadrozny, J. Telser and J. R. Long, *Polyhedron*, 2013, 64, 209–217; (b) F. Shao, B. Cahier, E. Riviere, R. Guillot, N. Guihery, V. E. Campbell and T. Mallah, *Inorg. Chem.*, 2017, 56, 1104–1111; (c) M. R. Saber and K. R. Dunbar, *Chem. Commun.*, 2014, 50, 12266–12269; (d) X.-N. Yao, M.-W. Yang, J. Xiong, J.-J. Liu, C. Gao, Y.-S. Meng, S.-D. Jiang, B.-W. Wang and S. Gao, *Inorg. Chem. Front.*, 2017, 4, 701–705.
- 19 H.-H. Cui, J. Wang, X.-T. Chen and Z.-L. Xue, Chem. Commun., 2017, 53, 9304-9307.
- J. Cho, R. Sarangi, H. Y. Kang, J. Y. Lee, M. Kubo, T. Ogura, E. I. Solomon and W. Nam, J. Am. Chem. Soc., 2010, 132, 16977-16986.
- (a) B. Cage, A. Hassan, L. Pardi, J. Krzystek, L. C. Brunel and N. S. Dalal, J. Magn. Reson., 1997, 124, 495-498; (b) A. Hassan, L. Pardi, J. Krzystek, A. Sienkiewicz, P. Goy, M. Rohrer and L. C. Brunel, J. Magn. Reson., 2000, 142, 300-312.
- 22 SMART & SAINT Software Reference Manuals, version 6.45; Bruker Analytical X-ray Systems, Inc.: Madison, WI, 2003.
- 23 G. M. Sheldrick, SADABS: Software for Empirical Absorption Correction, version 2.05; University of Göttingen: Göttingen, Germany, 2002.
- 24 G. M. Sheldrick, SHELXL-2014: Program for Crystal Structure Refinement; University of Göttingen: Göttingen, Germany, 2014.
- 25 G. A. Bain and J. F. Berry, *J. Chem. Educ.*, 2008, **85**, 532-536.
- 26 S. Khan, S. Sproules, L. S. Natrajan, K. Harms and S. Chattopadhyay, *New J. Chem.*, 2018, **42**, 1634—1641.
- 27 S. Alvarez, D. Avnir, M. Llunell and M. Pinsky, New J. Chem., 2002, 26, 996 – 1009.
- 28 (a) M. Llunell, D. Casanova, J. Cirera, P. Alemany and S. Alvarez, Shape Program, Version 2.1, 2013; (b) S. Alvarez, P. Alemany, D. Casanova, J. Cirera, M. Llunell and D. Avnir, Coord. Chem. Rev., 2005, 249, 1693-1708.
- 29 F. E. Mabbs, D. J. Machin, *Magnetism and Transition Metal Complexes*; Dover Publications: Mineola, NY, 2008.
- 30 (a) F. Lloret, M. Julve, J. Cano, R. Ruiz-García and E. Pardo, Inorg. Chim. Acta, 2008, 361, 3432-3445; (b) J. Titiš and R. Boča, Inorg. Chem., 2011, 50, 11838-11845.
- 31 N. F. Chilton, R. P. Anderson, L. D. Turner, A. Soncini and K. S. Murray, *J. Comput. Chem.*, 2013, **34**, 1164–1175.
- 32 (a) J. Krzystek, O. Ozarowski and J. Telser, Coord. Chem. Rev., 2006, 250, 2308–2324; (b) J. Krzystek, S. A. Zvyagin, O. Ozarowski, S. Trofimenko and J. Telser, J. Magn. Reson., 2006, 178, 174–183.

- 33 L. Banci, A. Bencibi, C. Benelli, D. Gatteschi and C. Zanchini, *Struct. Bonding*, 1982, 52, 37-86.
- 34 Simulations were performed using SPIN developed by Andrew Ozarowski at the National High Magnetic Field Laboratory, USA.
- 35 (a) R. L. Carlin, A. J. van Duyneveldt, Magnetic Properties of Transition Metal compounds, Springer-Verlag, New York, 1976; (b) K.N. Shrivastava, Phys. Status Solidi B, 1983, 117, 437-458.
- 36 (a) K. S. Cole and R. H. Cole, *J. Chem. Phys.*, 1941, **9**, 341–351; (b) Y. -N. Guo, G. -F. Xu, Y. Guo and J. Tang, *Dalton Trans.*, 2011, **40**, 9953-9963.
- 37 (a) R. Boča, J. Miklovič and J. Titiš, *Inorg. Chem.*, 2014, **53**, 2367-2369; (b) J. Miklovič, D. Valigura, R. Boča and J. Titiš, *Dalton Trans.*, 2015, **44**, 12484-12487; (c) Y. -L. Wang, L. Chen, C. -M. Liu, Y. -Q. Zhang, S. -G. Yin and Q. -Y. Liu, *Inorg. Chem.*, 2015, **54**, 11362-11368; (d) J. Li, Y. Han, F. Cao, R. -M. Wei, Y. -Z. Zhang and Y. Song, *Dalton Trans.*, 2016, **45**, 9279–9284.